Incorporation of technetium into spinel ferrites

Wayne W. Lukens,[1*] Nicola Magnani,[1,2] Tolek Tyliszczak,[3] Carolyn I. Pearce,[4] David K. Shuh[1]

1) Chemical Sciences Division, Lawrence Berkeley National Laboratory, Berkeley, CA 94720
2) European Commission, Joint Research Centre, Institute for Transuranium Elements, Karlsruhe
3) Advanced Light Source, Lawrence Berkeley National Laboratory, Berkeley, CA 94720
4) Geosciences Group, Pacific Northwest National Laboratory, Richland, WA 99354

* MS 70A-1150, Lawrence Berkeley National Laboratory, Berkeley, CA 94720. Phone (510) 486-4305; Fax (510) 486-5596. WWLukens@lbl.gov.

Abstract

Technetium (^{99}Tc) is a problematic fission product for the long-term disposal of nuclear waste due to its long half-life, high fission yield, and to the environmental mobility of pertechnetate, the stable species in aerobic environments. One approach to preventing ^{99}Tc contamination is using sufficiently durable waste forms. We report the incorporation of technetium into a family of synthetic spinel ferrites that have environmentally durable natural analogs. A combination of X-ray diffraction, X-ray absorption fine structure spectroscopy and chemical analysis reveals that Tc(IV) replaces Fe(III) in octahedral sites and illustrates how the resulting charge mismatch is balanced. When a large excess of divalent metal ions is present, the charge is predominantly

balanced by substitution of Fe(III) by M(II). When a large excess of divalent metal ions is absent, the charge is largely balanced by creation of vacancies among the Fe(III) sites (maghemitization). In most samples, Tc is present in Tc-rich regions rather than being homogeneously distributed.

Introduction

Technetium (^{99}Tc) is a problematic fission product for nuclear waste disposal due to its long half-life (211,000 yr), high fission yield (6 %), and to the environmental mobility of pertechnetate (TcO_4^-), the stable form in aerobic environments.[1-4] ^{99}Tc migration may be minimized by disposal in an anaerobic repository since Tc(IV) is stable under these conditions and is not highly mobile.[3] Alternatively, technetium may be immobilized in a waste form that is sufficiently durable to prevent release of ^{99}Tc until an acceptable fraction has decayed. The current U.S. high-level waste repository is Yucca Mountain, which is aerobic and oxidizing.[5] In addition, the majority of the ^{99}Tc from plutonium production at the Savannah River and Hanford Sites will be disposed in near-surface, aerobic repositories although the Savannah River Site facility will be reducing initially.[6,7] Disposal of ^{99}Tc in current and proposed aerobic repositories underscores the interest in durable waste forms for ^{99}Tc.

Even under reducing conditions, the 3 pM solubility of $TcO_2 \cdot xH_2O$ exceeds the EPA maximum contaminant level of 900 pCi/L or 0.5 pM.[8-10] Naturally occurring ligands can increase the solubility of Tc(IV).[11-14] Therefore, durable waste forms are also desirable for ^{99}Tc disposal in an anaerobic repository. The most commonly used waste form, borosilicate glass, is durable, but loss of volatile technetium species during glass vitrification can make it difficult to retain

technetium in the glass.[15-18] Alternatives include synthetic mineral phases, such as Synroc.[19] Likewise, certain mineral phases are both highly durable and could accommodate Tc doping.[20] The similarity of the six coordinate ionic radii of Tc(IV), Ti(IV), and Fe(III), 0.645 Å, 0.604 Å and 0.645 Å,[21] respectively, suggests that Tc(IV) can replace Ti(IV) or Fe(III) in an oxide mineral.[20] Rutile (TiO_2), hematite (α-Fe_2O_3) and goethite (α-FeOOH), are known to be durable under aerobic conditions.[22-26] Hematite and goethite are unstable under reducing conditions and could release ^{99}Tc; however, migration is slow under these conditions.[3] Moreover, Tc(IV) can be incorporated into mineral phases under these conditions as demonstrated by Kobayashi, et al. who showed that prolonged contact of magnetite (Fe_3O_4) with TcO_4^- leads to Tc(IV) incorporation.[27] Iron oxides, particularly goethite, have received attention as waste forms for stabilizing ^{99}Tc.[28,29] Other iron oxides can also accommodate Tc(IV). Pepper, et al., incorporated Tc(IV) into an iron oxide phase resulting from oxidation of green rust.[30] Marshall, et al. demonstrated that adsorption of Tc(IV) onto ferrihydrite followed by conversion to magnetite results in Tc doping.[31] Tc-doped magnetite has been studied computationally by Smith, et al..[32] Lee, at al. demonstrated that Tc(IV) may be incorporated into the lattice of transition metal doped magnetites.[18]

Another family of iron oxides, spinel ferrites (MFe_2O_4, where M is Mg(II), Mn(II), Co(II), or Ni(II)), especially nickel/magnesium ferrite, $Mg_xNi_{1-x}Fe_2O_4$, are highly durable as evidenced by their persistence since being deposited widely across earth's surface 65 million years ago by the Chixulub meteorite impact.[33] These minerals are inverse spinels, but they will be referred to as "spinel ferrites" for brevity. Synthetic spinel ferrites are attractive potential waste forms for several reasons. Aqueous synthesis conditions and short reaction times (few hours) make them

amenable to processing.[34-38] They are magnetic, potentially allowing magnetic separation of Tc. Incorporation of Tc(IV) into magnetite,[18,27,31] suggests that other Tc(IV)-doped spinel ferrites may be prepared. This observation leads the hypothesis that starting from TcO_4^-, Tc(IV) will be homogeneously incorporated into spinel ferrites by replacing Fe(III) on M_O sites provided that sufficient Fe(II) is present to reduce TcO_4^-.

To test the hypothesis and to understand the factors controlling Tc incorporation into spinel ferrites, we have prepared: (i) a series of Tc(IV)-doped spinel ferrites with the composition $Tc_{0.1}M_{1.1}Fe_{1.8}O_4$, where M is Mn, Co, and Ni; and (ii) a series of magnetites doped with Tc(IV) and divalent metals having the composition $Tc_{0.1}M_{0.2}Fe_{2.7}O_4$ where M is Mg, Mn, Fe, Co, and Ni. The objectives of this study were (i) to determine whether Tc could be incorporated into the octahedral sites (M_O) of spinel ferrites, $M_xFe_yO_4$, (ii) to determine the effect of ionic radius of the divalent metal ion, M, on the incorporation of Tc in the spinel ferrite lattice, and (iii) to determine the effect of different synthetic routes on the incorporation of Tc. The two synthetic routes examined were the traditional coprecipitation route (samples indicate by "-c"),[34] in which a mixture of M(II), Fe(II) and Fe(III), and TcO_4^- is treated with NaOH to form the ferrite spinel and a oxidation route (samples indicated by "-o") in which a mixture of M(II), Fe(II) and TcO_4^- is treated with NaOH and $NaNO_3$, and Fe(III) is generated *in situ* by oxidation of Fe(II) by NO_3^-.[36]

Experimental Details

Caution: ^{99}Tc is β−emitter. All operations were carried out in a laboratory equipped to handle this isotope.

General. Water was deionized using a Milli-Q Gradient A-10 system. Chemicals were ACS grade or better and were used as received. Fe(II)/total Fe ratios (Fe(II)/ΣFe) in the spinels were determined colorimetrically.[39,40] In this method, V(V) is reduced to V(IV) by Fe(II) during dissolution of the sample in acid. When 2,2'-bipyridyl (bipy) and buffer are added, V(IV) quantitatively reduces $Fe(bipy)_3^{3+}$ to red $Fe(bipy)_3^{2+}$, which is measured spectrophotometrically. The Fe(II)/ΣFe ratios for the Tc-doped samples were decreased proportionally to the amount of Tc recovered from the spinel ferrites and the Tc/Fe ratio to account for reduction of three V(V) by each Tc(IV), e.g., for $Tc_{0.1}Mn_{1.1}Fe_{1.8}O_4$-o Fe(II)/ΣFe was decreased by 3 (e^-/Tc(IV)) × 0.99 (Tc recovered from solid) × 0.1/1.8 (Tc/Fe). Two sets of independently prepared samples were used for characterization. The initial set was used for XRD and XAFS studies. Later, a second set was prepared for LSC and Fe(II)/Fe(III) measurements to address questions that arose during the analysis of the XRD and XAFS results. Both sets were prepared using the same procedures.

Synthesis of Tc-doped spinel ferrites

Note: The stoichiometry of the samples (e.g., "$Tc_{0.1}Co_{1.1}Fe_{1.8}$") are based on the amount of each metal added during the synthesis. The samples contain 4 wt% Tc.

Two approaches were used to prepare samples: coprecipitation and oxidation. In the coprecipitation approach, TcO_4^- was added to a mixture of divalent metal ion and Fe(III).[34] A five-fold excess of Fe(II) relative to TcO_4^- was used to reduce TcO_4^- to Tc(IV). The solution was neutralized with sodium hydroxide and heated. These samples are indicated by a "c" after the

formula, e.g., $Tc_{0.1}Fe_{2.9}O_4$-c. In the oxidation route, TcO_4^- was added to a mixture of Fe(II) and a divalent metal ion; sodium hydroxide and sodium nitrate were added and the solution was heated.[36] Fe(III) is formed *in situ* through oxidation of Fe(II) by nitrate, hence the term "oxidation route." These samples are indicated by an "o" after the formula, e.g., $Tc_{0.1}Fe_{2.9}O_4$-o. Following the synthesis, the samples were handled and stored in air, and no attempts were made to exclude oxygen.

Coprecipitation (adapted from ref 33)**.** $CoCl_2$•$6H_2O$ (53 mg, 0.22 mmol) was dissolved in a mixture of 1.0 M $FeSO_4$ (0.10 mL, 0.10 mmol) and 1.0 M $NH_4Fe(SO_4)_2$ (0.26 mL, 0.26 mmol). The solution was sparged with argon for 1 minute. A 0.10 M solution of TcO_4^- in 0.03 M HNO_3 (200 uL, 0.02 mmol) was added. The headspace of the tube was purged with argon, and the tube was vigorously shaken. Aqueous 2.00 M NaOH (0.91 mL, 1.81 mmol OH^-) was added. The headspace of the tube was purged with argon, and the tube was vigorously shaken. The tube was heated to 95 °C for 90 minutes. After heating, the tube was centrifuged (5 min, 8500 g) and the solution decanted. The black solid was washed with 2×1.5 mL water and 1.5 mL acetone.

Oxidation (adapted from ref. 35). $CoCl_2$•$6H_2O$ (53 mg, 0.22 mmol) was dissolved in 1.0 M $FeSO_4$ (0.36 mL, 0.36 mmol). The solution was sparged with argon for 1 minute. A 0.11 M solution of TcO_4^- in 0.03 M HNO_3 (200 uL, 0.02 mmol) was added. The headspace of the tube was purged with argon, and the tube was vigorously shaken. An aqueous solution of 1.00 M $NaNO_3$ and 2.00 M NaOH (0.61 mL, 1.21 mmol OH^-) was added. The headspace of the tube was purged with argon, and the tube was vigorously shaken. The tube was heated to 95 °C for 90

minutes. After heating, the tube was centrifuged (5 min, 8500 g), and the supernate decanted. The black solid was washed in air with 2×1.5 mL water and 1.5 mL acetone.

Synthesis of undoped spinel ferrites. Samples with the same transition metal composition, but without added Tc were prepared. Both the oxidation synthesis and coprecipitation synthesis were performed as described above except that 200 uL of water was used in place of the NH_4TcO_4 solution.

Liquid Scintillation Counting (LSC). Solutions were centrifuged (5 min, 8500 g) to remove Tc-doped ferrite nanoparticles. 100 uL of this solution was added to 4 mL of Ecolume. Samples were analyzed using a Wallac 1414 liquid scintillation counter. Results are not corrected for chemical quench. Comparison of the spectral quench parameter, SQP(E), to a ^{99}Tc quench curve prepared using nitromethane showed that quenching was less than 1%.

X-ray diffraction (XRD). An acetone suspension of the sample was dropped onto a silicon zero background plate. Samples were sealed with Kapton film to control contamination. Diffractograms were recorded using a Panalytical X'Pert Pro diffractometer with a Cu source and a silicon strip detector except for sample $Tc_{0.1}Ni_{0.2}Fe_{2.7}O_4$-c, which was recorded using a Co source. Data were summed and analyzed using HiScore Plus software. A blank diffraction pattern from the zero background plate and the Kapton film was subtracted from each diffraction pattern. An empirical background consisting of a curve through the bases of the peaks at low 2θ and through the baseline at high 2θ was removed. The diffraction data were modeled using the

157 crystal structure of magnetite. Rietveld refinement using X'Pert High Score Plus was used to
158 determine the lattice parameters and to estimate the sizes of the crystallites.
159
160 **X-ray absorption fine structure (XAFS) measurements**. Samples were dispersed in acetone or
161 water and centrifuged (5 min, 8500 g), and the liquid was discarded to produce a homogeneous
162 pellet. Data was obtained at room temperature at the Tc K-edge on Beamline 11-2 or 4-1 of the
163 Stanford Synchrotron Radiation Lightsource. Most data were obtained during a single
164 experiment. For samples $Tc_{0.1}Co_{1.1}Fe_{1.8}O_4$-o, $Tc_{0.1}Mg_{0.2}Fe_{2.7}O_4$-o, and $Tc_{0.1}Ni_{0.2}Fe_{2.7}O_4$-c, the
165 pellet dried out and disintegrated inside the centrifuge tube. Spectra from these samples were re-
166 collected during a subsequent experiment using freshly prepared material. X-rays were
167 monochromatized using a double-crystal monochromator with Si [220] $\phi = 90$ crystals; the
168 second crystal was detuned by 70% to reduce the harmonic content of the beam. Spectra were
169 recorded in transmission mode using argon filled ion chambers.
170
171 Data were analyzed by standard procedures[41] using ifeffit[42] and Artemis/Athena.[43] Theoretical
172 scattering curves were calculated using Feff6[44] based on the structure of titanomagnetite
173 ($Ti_{0.1}Fe_{2.9}O_4$) with Tc in the octahedral site.[45] Coordination numbers for the neighboring atoms
174 were fixed at the values found in the crystal structure except for the oxygen shell at 2 Å. This
175 shell was split into two shells, one with a short distance (1.5 to 1.75 Å) and another with a longer
176 distance (2 Å); the sum of the oxygen coordination numbers for these shells was fixed at 6, the
177 number of oxygen nearest neighbors for the Ti(IV) site in titanomagnetite. The value of S_0^2 was
178 determined to be 0.80 (rather than 0.90) for fitting the data in this study by fitting several
179 extended X-ray absorption fine structure (EXAFS) spectra of the TcO_4^- reference collected

simultaneously with the data. The statistical significance of each scattering shell was evaluated using an F-test.[46]

X-ray magnetic circular dichroism spectroscopy (XMCD). Sample was placed on a 100 nm thick Si_3N_4 window, which was sealed to an identical Si_3N_4 window with epoxy. Data was recorded at the Molecular Environmental Science Beamline 11.0.2 at the Advanced Light Source (ALS) with a scanning transmission X-ray microscope (STXM). XMCD spectra were recorded at the Fe $L_{2,3}$-edge with the sample in a 0.5 T magnetic field using left and right circularly polarized X-rays from an elliptically polarizing undulator.[47] Data were recorded as images obtained at different X-ray energies. The background data was obtained from the portion of the image with no sample. Data were pre- and post-edge normalized. Data were fit using nonlinear least-squares analysis with calculated spectra[48,49] for each site as previously described[50,51]

Results and discussion

Incorporation of Tc into spinel ferrites.

Incorporation of TcO_4^- was evaluated by LSC analysis of the solution remaining after preparation of the spinel ferrite (Table S1). More than 99.5 % of the Tc was removed from solution in all cases; in the oxidation route, more than 99.88 % of the Tc was removed. The Tc remaining is solution is presumably TcO_4^-. These results are consistent with work by Livens and coworkers using green rust to trap TcO_4^-.[30] Other studies showed that iron metal, magnetite, and adsorbed Fe(II) can effectively remove TcO_4^- from solution.[27,52-56] Recovery of Tc from the spinel ferrites was determined during analysis of Fe(II) and total iron (ΣFe) by determining the amount of ^{99}Tc using LSC. The recovery of Tc varied from 81% to 100% (Table S1).

X-ray diffraction (XRD). Tc-doped spinel ferrites were characterized using XRD to determine the oxide phases present, the lattice parameters, and the crystallite sizes of the major phase. XRD patterns and Rietveld fits for the Tc-doped spinel ferrites are given in Figure 1. Samples prepared by the coprecipitation route have broader peaks than samples produced by the oxidation route due to the smaller crystallites produced by more rapid nucleation of nanoparticles in the coprecipitation synthesis.[57] These results are consistent with the original magnetite syntheses from which the procedures to prepare Tc-doped spinel ferrites were adapted.[34,36] Undoped spinel ferrites, prepared under identical conditions, but adding water instead of TcO_4^-, were also characterized. These undoped samples allow the effect of Tc doping on the lattice parameters and Fe(II)/ΣFe to be determined.

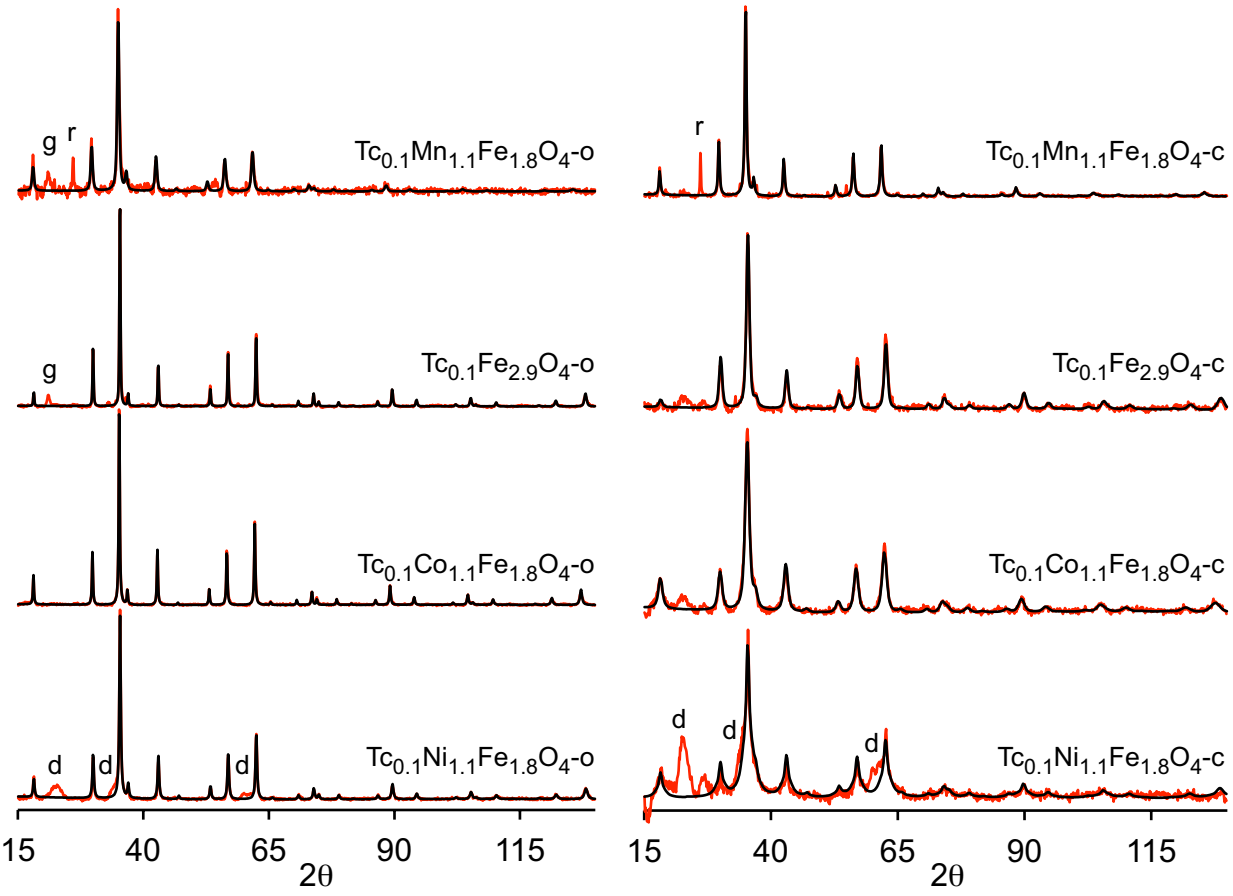

215

216 **Figure 1:** X-ray powder patterns (in red) and Rietveld fits (black) of spinel ferrites. Data are
217 normalized so that the largest peaks have the same height. Data for $Tc_{0.1}M_{0.2}Fe_{2.7}O_4$ are given in
218 the SI and are similar to those of $Tc_{0.1}Fe_{2.9}O_4$. Impurity peaks are labeled with g for goethite, r
219 for α-MnOOH, and d for the layered double hydroxide. Diffraction peaks of the coprecipitation
220 samples are broader than those produced by the oxidation route due to the smaller crystallite
221 sizes of the coprecipitation samples.

222

223 The major phase was spinel ferrite in all samples. The most common impurity was goethite,
224 which forms in the presence of oxygen.[36] Its presence suggests that the short sparging period did
225 not remove all of the oxygen. When Mn(II) was used, α-MnOOH, was observed. When Ni(II)

226 was used, an impurity was indicated by broad peaks at 2θ = 22.5°, 35°, and 60°, which is
227 consistent with the presence of a lamellar nickel/iron layered double hydroxide (LDH) phase.[58,59]
228
229 **Effects of charge compensation on lattice parameters and Fe(II)/ΣFe ratio.** Tc-doping
230 affects the lattice parameters of the spinel ferrites (Figure 2), which provides information about
231 the mechanism that balances the charge mismatch created when Tc(IV) replaces Fe(III). While
232 other mechanisms are possible,[32] the charge mismatch may be balanced in two main ways: M(II)
233 could replace Fe(III) (divalent substitution) or one vacancy at a Fe(III) site could be created for
234 every three Tc(IV) (maghemitization). In $TiFe_2O_4$ (ulvöspinel), the charge mismatch is balanced
235 by divalent substitution leading to a lattice expansion to 8.521 Å relative to magnetite, 8.397 Å.[45]
236 Lattice expansion occurs because M(II) ions are larger than the Fe(III) that they replace. In
237 contrast, maghemitization decreases the lattice parameter, i.e. to 8.341 Å in of Ti-doped
238 maghemite, $Ti_{0.42}Fe_{2.18}O_4$.[60] Previous studies of iron oxides doped with tetravalent ions suggest
239 that divalent substitution occurs under reducing conditions and maghemitization occurs under
240 oxidizing conditions.[61-64]
241
242 The lattice parameters of the Tc-doped and undoped spinel ferrites are compared in Figure 2. To
243 explain the results, the samples are categorized by the amount of M(II) and Fe(II) present during
244 synthesis. Samples prepared by the oxidation route are "high Fe(II)" while coprecipitation
245 samples are "low Fe(II)". Spinel ferrites, $Tc_{0.1}M_{1.1}Fe_{1.8}O_4$, are "high M(II)," and doped magnetite
246 samples, $Tc_{0.1}M_{0.2}Fe_{2.7}O_4$, are "low M(II)." For example, $Tc_{0.1}Co_{1.1}Fe_{1.8}O_4$-c is high M(II), low
247 Fe(II). In samples with high M(II) and/or high Fe(II), Tc-doping increases the lattice parameters
248 with the exception of $Tc_{0.1}Co_{1.1}Fe_{1.8}O_4$-c and $Tc_{0.1}Fe_{2.9}O_4$-o. The increased lattice parameter in

these samples suggests that charge is mainly balanced by divalent substitution, which is consistent with the large excess of divalent metal ions, either M(II) or Fe(II), present during these syntheses. On the other hand, except for $Tc_{0.1}Ni_{0.2}Fe_{2.7}O_4$-c and $Tc_{0.1}Mn_{0.2}Fe_{2.7}O_4$-c, samples with low M(II) and low Fe(II) show a decrease in the lattice parameter upon Tc-doping. This decrease suggests that the charge mismatch is predominantly balanced by maghemitization, which is consistent with the smaller amounts of divalent metal ions present during synthesis.

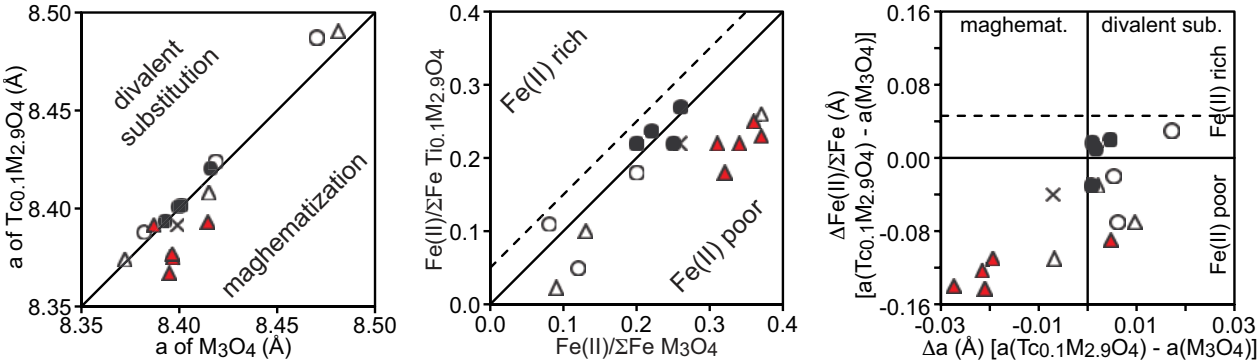

Figure 2. (Left panel) comparison of lattice parameters of Tc doped spinel ferrites (vertical axis) with the lattice parameters of undoped samples (horizontal axis) (left). (Center) comparison of the Fe(II)/total Fe values for Tc-doped spinel ferrites (vertical axis) with the undoped analogs (horizontal axis). (Right) Change in Fe(II)/ΣFe (vertical axis) and lattice parameter (horizontal axis) as a result of Tc-doping. The dashed line indicates the Fe(II)/total Fe value for a Tc-doped spinel ferrite if the charge is balanced by replacing Fe(III) by Fe(II). Open circles: $Tc_{0.1}M_{1.1}Fe_{1.8}O_4$-o (high M(II), high Fe(II)). Filled circles: $Tc_{0.1}M_{0.2}Fe_{2.7}O_4$-o (low M(II), high Fe(II)). Open triangles: $Tc_{0.1}M_{1.1}Fe_{1.8}O_4$-c (high M(II), low Fe(II)). Filled triangles: $Tc_{0.1}M_{0.2}Fe_{2.7}O_4$-c (low M(II), low Fe(II)).

The XRD data suggests that the charge mismatch created by Tc doping is predominantly balanced by divalent substitution in high Fe(II) or high M(II) samples. The identity of the

267 divalent cation may be inferred from the ratio of Fe(II) to total iron (Fe(II)/ΣFe) (Table S1 and
268 Figure 2). If the divalent cation is Fe(II), Fe(II)/ΣFe will increase upon Tc doping as determined
269 by stoichiometry (dashed lines in Figure 2 for $Tc_{0.1}Fe_{2.9}O_4$). With some exceptions, Fe(II)/ΣFe is
270 smaller for Tc-doped samples, indicating that M(II) rather than Fe(II) replaces Fe(III) during
271 divalent substitution in the high M(II) samples. The relationship between the change in lattice
272 parameter and change in Fe(II)/ΣFe is illustrated in the right panel of Figure 2. In the low M(II)
273 samples (filled symbols) the changes in lattice parameter and Fe(II)/ΣFe are generally correlated
274 since either Fe(II) replaces Fe(III) to balance the charge and expand the lattice or the samples are
275 maghemitized and the lattice shrinks. High M(II) samples show less correlation because
276 replacing Fe(III) by M(II) expands the lattice but has little effect on Fe(II)/ΣFe.
277
278 **XAFS results.** Representative Tc K-edge XANES and EXAFS spectra are shown in Figures 3
279 and 4, respectively (the other EXAFS spectra are similar to $Tc_{0.1}Fe_{2.9}O_4$-o and are included in the
280 SI). The model used to fit the EXAFS spectra is the octahedral site (M_O) of titanomagnetite
281 ($Ti_{0.1}Fe_{2.9}O_4$) occupied by Ti(IV). Tc(IV) and Ti(IV) are similar in size, so the local structure of
282 Ti(IV) in the M_O site is an appropriate model for the structure of Tc(IV) in spinel ferrites.
283 Coordination numbers for the metal neighbors were fixed at the value in the crystal structure, e.g.
284 6 nearest octahedral site (M_O) neighbors. A minor contribution from a short Tc-O distance at
285 either <1.7 Å or ~ 1.72 Å was used to obtain the best fit (Table 1). The 1.72 Å Tc-O distance is
286 consistent with TcO_4^-.[65] The shorter Tc-O distance is ascribed to a fitting artifact. In some cases,
287 the shorter Tc-O distance is consistent with the distance of a terminal oxo group of Tc(V), 1.64
288 Å.[66] However, the shorter Tc-O distance varies widely from 1.51 Å to 1.69 Å. This variation is
289 inconsistent with the presence of a well-defined Tc(V) species for which the same Tc-O distance

should be observed in all samples as seen in the samples that contain TcO_4^-. Moreover, XANES analysis, Table 1, does not confirm the presence Tc(V) in any of the samples with very short Tc-O distances. Only two samples contain Tc(V) greater than 3σ in the XANES analysis: $Tc_{0.1}Mn_{1.1}Fe_{1.8}O_4$-c and $Tc_{0.1}Ni_{1.1}Fe_{1.8}O_4$-c, and both have Tc-O bond distances consistent with TcO_4^-. In contrast, EXAFS and XANES analysis show better agreement for TcO_4^-. In all cases but one, TcO_4^- is found in materials produced by the low Fe(II), coprecipitation route. For most samples produced by the oxidation route, the only significant oxidation state is Tc(IV), presumably due to the large excess of Fe(II) used in these syntheses. Based on the XANES analyses, the main oxidation state of Tc in all samples is Tc(IV) although some contain TcO_4^-.

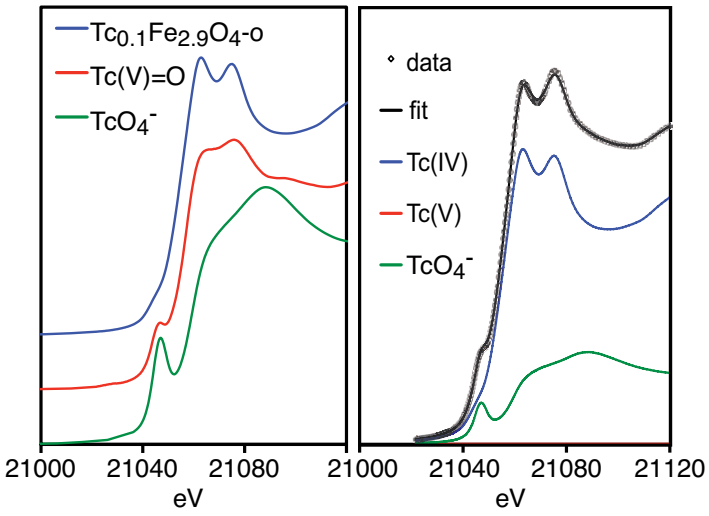

Figure 3. XANES standard spectra (left) and deconvoluted XANES fit for $Tc_{0.1}Co_{1.1}Fe_{1.8}O_4$-c (right).

304 **Table 1:** Tc oxidation state distribution from EXAFS and XANES analyses

Sample[a]	Tc-O (Å) (EXAFS)	# short Tc-O[b] (EXAFS)	TcO_4^-[c] (EXAFS)	Tc(IV) (XANES)	Tc(V)[d] (XANES)	TcO_4^- (XANES)
$Tc_{0.1}Mn_{1.1}Fe_{1.8}O_4$-o	1.59(1)	0.28(8)	--	1.0(1)	0.0(2)	0.00(6)
$Tc_{0.1}Co_{1.1}Fe_{1.8}O_4$-o	1.54(3)	0.3(1)	--	1.0(1)	0.0(2)	0.00(6)
$Tc_{0.1}Ni_{1.1}Fe_{1.8}O_4$-o	1.79(3)	--	0.10(2)	0.96(8)	0.0(1)	0.04(4)
$Tc_{0.1}Mg_{0.2}Fe_{2.7}O_4$-o	1.54(2)	0.29(9)	--	1.00(9)	0.0(1)	0.00(4)
$Tc_{0.1}Mn_{0.2}Fe_{2.7}O_4$-o	1.51(1)	0.38(9)	--	0.93(5)	0.00(8)	0.07(3)
$Tc_{0.1}Fe_{2.9}O_4$-o	1.61(2)	0.20(8)	--	1[e]		
$Tc_{0.1}Co_{0.2}Fe_{2.7}O_4$-o	1.66(2)	0.4(1)	--	0.9(1)	0.0(2)	0.10(6)
$Tc_{0.1}Ni_{0.2}Fe_{2.7}O_4$-o	1.57(1)	0.31(8)	--	1.00(6)	0.0(1)	0.00(3)
$Tc_{0.1}Mn_{1.1}Fe_{1.8}O_4$-c	1.72(1)	--	0.10(2)	0.62(9)	0.4(1)	0.01(5)
$Tc_{0.1}Co_{1.1}Fe_{1.8}O_4$-c	1.718(5)	--	0.21(2)	0.75(5)	0.00(7)	0.25(3)
$Tc_{0.1}Ni_{1.1}Fe_{1.8}O_4$-c	1.726(6)		0.30(2)	0.54(3)	0.24(5)	0.22(2)
$Tc_{0.1}Mg_{0.2}Fe_{2.7}O_4$-c	1.671(6)	0.33(8)	--	0.84(3)	0.11(4)	0.06(1)
$Tc_{0.1}Mn_{0.2}Fe_{2.7}O_4$-c	1.715(7)		0.18(2)	0.80(3)	0.04(4)	0.16(2)
$Tc_{0.1}Fe_{2.9}O_4$-c	1.63(1)	0.29(6)	--	0.89(3)	0.09(5)	0.03(2)
$Tc_{0.1}Co_{0.2}Fe_{2.7}O_4$-c	1.716(9)		0.19(2)	0.82(3)	0.01(4)	0.17(1)
$Tc_{0.1}Ni_{0.2}Fe_{2.7}O_4$-c	1.720(8)		0.15(2)	0.82(2)	0.00(3)	0.18(1)

305 a) Samples with an "o" suffix were prepared by oxidation; "c" by coprecipitation
306 b) Coordination number of the O neighbors with a Tc-O distance <1.7 Å.
307 c) Fraction of TcO_4^- is ¼ of the number of O neighbors with a Tc-O distance between 1.7
308 and 1.8 Å.
309 d) Relative to sample $Tc_{0.1}Fe_{2.9}O_4$-o.
310 e) The XANES spectrum of this sample is the Tc(IV) standard.
311

312

313

Table 2. Local environment of Tc in spinel ferrites from EXAFS[a,b]

Sample[a]	6 O (Å)	σ^2 (Å^2)	6 M_O (Å)[c]	# of Tc[d]	σ^2 (Å^2)	6 M_T (Å)[e]	σ^2 (Å^2)	12 M_O (Å)[b]
M_O site in Fe_3O_4	2.06	--	2.97	--	--	3.48	--	5.15
M_O site in $TiFe_2O_4$[45]	2.09	--	3.02	--	--	3.54	--	5.22
High M(II), High Fe(II)								
$Tc_{0.1}Mn_{1.1}Fe_{1.8}O_4$-o	2.025(3)	0.004	3.087(7)	2.0(1)	0.004	3.565(8)	0.013	5.27(2)
$Tc_{0.1}Co_{1.1}Fe_{1.8}O_4$-o	2.009(4)	0.003	3.035(5)	0[f]	0.006	3.517(7)	0.006	5.19(1)
$Tc_{0.1}Ni_{1.1}Fe_{1.8}O_4$-o	2.009(4)	0.003	3.034(6)	1.2(5)	0.003	3.514(7)	0.007	5.19(1)
Low M(II), High Fe(II)								
$Tc_{0.1}Mg_{0.2}Fe_{2.7}O_4$-o	2.034(4)	0.003	3.096(9)	1.9(2)	0.004	3.537(7)	0.007	5.22(2)
$Tc_{0.1}Mn_{0.2}Fe_{2.7}O_4$-o	2.036(4)	0.004	3.100(8)	2.20(8)	0.002	3.53(1)	0.010	5.25(2)
$Tc_{0.1}Fe_{2.9}O_4$-o	2.027(3)	0.004	3.090(7)	2.1(1)	0.004	3.524(6)	0.008	5.22(2)
$Tc_{0.1}Co_{0.2}Fe_{2.7}O_4$-o	2.026(6)	0.005	3.08(1)	2.2(1)	0.003	3.51(1)	0.008	5.20(2)
$Tc_{0.1}Ni_{0.2}Fe_{2.7}O_4$-o	2.030(3)	0.003	3.075(7)	1.9(1)	0.003	3.530(6)	0.007	5.21(1)
High M(II), Low Fe(II)								
$Tc_{0.1}Mn_{1.1}Fe_{1.8}O_4$-c	2.016(5)	0.004	3.083(1)	2.0(2)	0.003	3.550(3)	0.015	5.26(4)
$Tc_{0.1}Co_{1.1}Fe_{1.8}O_4$-c	2.027(5)	0.004	3.069(8)	2.07(8)	0.001	3.54(1)	0.011	5.23(2)
$Tc_{0.1}Ni_{1.1}Fe_{1.8}O_4$-c	2.027(8)	0.006	3.10(2)	2.3(2)	0.005	3.50(3)	0.018	f
Low M(II), Low Fe(II)								
$Tc_{0.1}Mg_{0.2}Fe_{2.7}O_4$-c	2.027(8)	0.005	3.10(2)	2.27(8)	0.003	3.51(3)	0.012	5.23(1)
$Tc_{0.1}Mn_{0.2}Fe_{2.7}O_4$-c	2.019(4)	0.005	3.083(7)	2.10(8)	0.003	3.509(9)	0.012	5.23(2)
$Tc_{0.1}Fe_{2.9}O_4$-c	2.020(3)	0.005	3.086(6)	2.17(6)	0.002	3.511(8)	0.011	5.23(2)
$Tc_{0.1}Co_{0.2}Fe_{2.7}O_4$-c	2.020(5)	0.005	3.077(9)	2.16(9)	0.003	3.51(1)	0.011	5.22(2)
$Tc_{0.1}Ni_{0.2}Fe_{2.7}O_4$-c	2.019(5)	0.005	3.074(9)	1.93(4)	0.004	3.509(9)	0.011	5.21(2)

a)

b) Standard deviations are given in parentheses in the same units as the last digit

c) M_O: octahedral sites

d) # of nearest octahedral neighbor that are Tc rather than Fe, Mg, Mn, Co, Ni

e) M_T: tetrahedral sites

f) Inclusion of this set of atoms did not improve the fit.

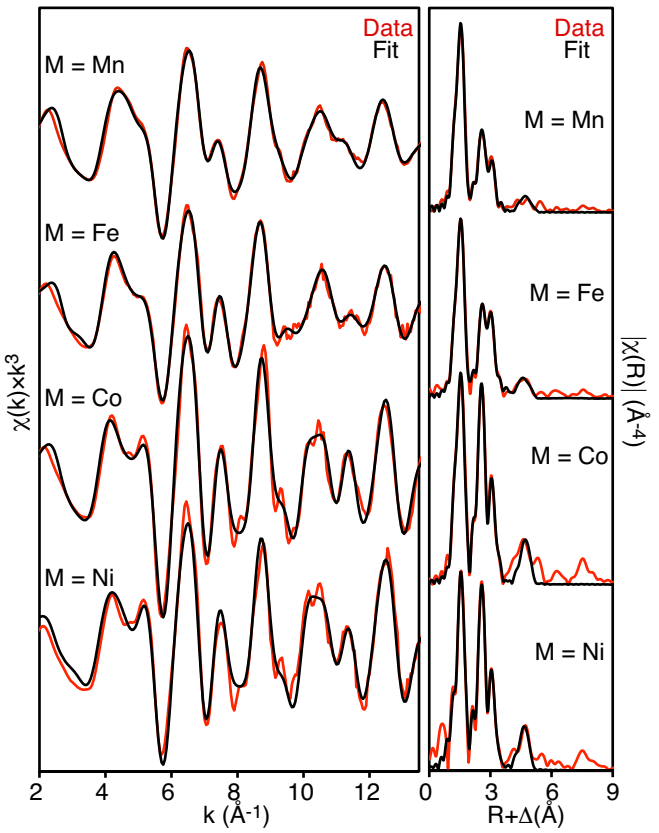

Figure 4. Tc K-edge EXAFS spectra of $Tc_{0.1}M_{1.1}Fe_{1.8}O_4$-o (left) and Fourier transforms (right). Data are shown in color and EXAFS fits are shown in black. The spectra of $Tc_{0.1}M_{0.2}Fe_{2.7}O_4$ are similar to that labeled M = Fe.

The EXAFS results, Table 2, are consistent with the bulk of Tc in the sample existing as Tc(IV) occupying the octahedral spinel site (M_O) site as previously seen for Tc-doped magnetite.[27,31] The local environment of Tc is more similar to the M_O site of ulvöspinel ($TiFe_2O_4$) than that of Fe_3O_4 as shown in Table 2. The oxygen neighbors at 2.0 Å are characteristic for Tc(IV) octahedrally coordinated by oxygen.[67] The Tc and Fe atoms at 3.1 Å are consistent with the six, edge-sharing M_O neighbors at 3.02 Å in $TiFe_2O_4$. The six Fe atoms at 3.5 Å are in agreement with the six, corner-sharing M_T neighbors at 3.53 Å in $TiFe_2O_4$. Scattering from more distant iron M_O sites at 5.2 Å was observed in most cases, which is consistent with the next-nearest

neighbor M_O sites at 5.22 Å in $TiFe_2O_4$. In some samples, scattering from more distant atoms can be observed at ~8 Å in the Fourier transformed spectra, which presumably corresponds to 42 Fe neighbors that are 7.9 and 8.2 Å from M_O. The presence of Fe and/or Tc neighbors[27] at 3.1 Å, 3.5 Å, and 5.2 Å is sufficient to show that the bulk of the Tc is doped into the M_O site. This result is consistent with previous EXAFS studies of magnetite doped with Sn(IV) or Ti(IV) and to the previously mentioned results for Tc(IV) doped magnetite.[62,68,69]

The most surprising result is that Tc is strongly clustered, which was not previously observed, presumably because the Tc/Fe ratio was much lower in those studies. At the doping level used here, each Tc would have 0.3 Tc neighbors if Tc were homogeneously distributed. Instead, each Tc has ~2 Tc neighbors. The local environment of Tc again resembles that of Ti in $TiFe_2O_4$ where each Ti has 3 Ti(IV) M_O neighbors, and the remaining M_O and M_T sites are occupied by Fe(II). The level of Tc clustering in the Tc-doped spinel ferrites implies that the M_O sites surrounding each Tc site contain approximately two Tc(IV) and four M(II) and that the neighboring M_T sites contain approximately three Fe(III) and three M(II).

The distances determined by EXAFS are slightly different from those determined by crystallography because EXAFS measures the local structure of Tc while XRD measures the average structure. The 2.02 Å Tc-O distance is shorter than M_O-O distance in $TiFe_2O_4$, which includes both Ti(IV)-O and Fe(II)-O distances. Using the ionic radius of four coordinate O^{2-} (1.24 Å),[21] the Tc-O distance is predicted to be 2.025 Å. In $TiFe_2O_4$, the average radius of M_O is 0.832 Å, and the predicted M_O-O distance is 2.07 Å. The longer Tc-M_O distance relative to $TiFe_2O_4$ largely results from Tc clustering. Each Tc has ~2 Tc neighbors and ~4 M(II) neighbors.

In $Tc_{0.1}Fe_{2.9}O_4$-o, the average ionic radius of the M_O neighbors of Tc is 0.875 Å, about 0.04 Å larger than in $TiFe_2O_4$, so the Tc-M_O distance determined by EXAFS should be longer than that determined by diffraction.

Fe L-edge XMCD spectroscopy. $Tc_{0.1}Fe_{2.9}O_4$-o was studied using XMCD at the Fe $L_{2,3}$-edge in an attempt to determine the distribution of Fe(II) and Fe(III) on the octahedral and tetrahedral sites. This technique has been widely used to study substituted magnetites including titanomagnetites.[50,51,68] The normal contrast X-ray image and the XMCD spectrum are shown in Figure 5. The cation distribution from the fit, normalized for 2.9 Fe and an M_T occupancy of 1, shows that the M_O sites contain 0.7 Fe(III) and 1.2 Fe(II) and M_T contains 1 Fe(III). This occupancy is similar to that predicted if the charge is balanced by diamagnetic substitution (M_O sites contain 0.1 Tc(IV), 0.8 Fe(III) and 1.1 Fe(II), and M_T sites contain 1 Fe(III)). The XMCD results suggest a Fe(II)/ΣFe ratio of 0.4, which is somewhat larger than measured colorimetrically, 0.21(1).

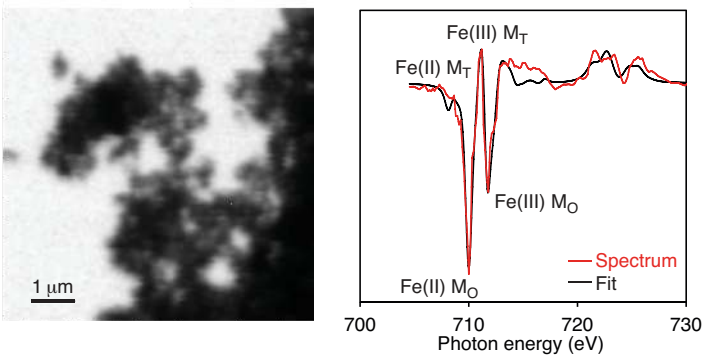

372

373 **Figure 5**. Normal contrast X-ray micrograph (STXM, left) of $Tc_{0.1}Fe_{2.9}O_4$-o illustrating the small
374 particle size. X-ray magnetic circular dichroism spectrum (XMCD, right) of $Tc_{0.1}Fe_{2.9}O_4$-o
375 obtained at the Fe $L_{2,3}$-edge. The XMCD spectrum is the difference between absorption of right
376 and left circularly polarized X-rays when the sample is in a magnetic field.

377

378 The Tc-doped spinel ferrites consist of Tc-rich regions and Tc-poor regions. This behavior
379 closely mirrors that of titanomagnetite where Ti(IV) mainly replaces Fe(III) on M_O, and the
380 charge is balanced by divalent substitution. Ti(IV) is homogeneously distributed above 600 °C.[70]
381 At lower temperatures, titanomagnetite undergoes spinodal decomposition forming titanium-
382 poor regions that resemble magnetite and titanium-rich regions that resemble ulvöspinel.[70]
383 Recent work by Lilova, et al. shows that the enthalpy of mixing for the ulvöspinel/magnetite
384 system is positive, consistent with the observed spinodal decomposition.[71] The behavior of the
385 Tc-doped spinel ferrites appears to be similar, and may explain why the local structure of Tc(IV)
386 more closely resembles ulvöspinel than magnetite.

387

388 **Implications for durability of Tc-doped spinels.** The spinel ferrites in this study are effective
389 at stabilizing Tc(IV) in the solid state and preventing its oxidation to TcO_4^-. Only the initial step
390 of the synthesis was performed under inert atmosphere. All subsequent operations, including

391 washing, storage, and spectroscopic studies, were performed in air. Nevertheless, Tc remained in
392 the reduced state. While the ability to stabilize Tc(IV) is necessary for these materials to be
393 effective waste forms for ^{99}Tc, the spinel ferrite matrix also must be sufficiently durable towards
394 dissolution or alteration.
395
396 The main concern, therefore, is the durability of the Tc-doped spinel ferrites. As prepared herein,
397 these materials are nanoparticles with high specific surface areas. In addition, the materials
398 contain Fe(II), which may adversely affect their durability. The effect of Fe(II) on durability is
399 best illustrated by magnetite and titanomagnetite. In aerobic environments, these materials are
400 oxidized to γ-Fe_2O_3 (maghemite) and titanomaghemite, respectively.[69,72] This transformation is
401 topotactic and unlikely to release doped Tc, as observed by Marshall et al.[31] While somewhat
402 durable, maghemite is unstable with respect to transformation to hematite or goethite. This
403 transformation is not topotactic and could lead to the loss of Tc to the environment. Work by
404 Um, et al. suggest that Tc(IV) can still trapped in goethite during the oxidation of magnetite.[28,29]
405 As in magnetite, the Fe(III) site in goethite is octahedral, and Tc(IV) can replace Fe(III) provided
406 that the charge mismatch is balanced. Ultimately, the best approach for determining how well
407 these materials immobilize ^{99}Tc is measuring the release of ^{99}Tc when these materials are re-
408 suspended in water.
409
410
411 **Acknowledgement**
412 This work (WWL, DKS, NM) was supported by the U.S. Department of Energy, Office of
413 Science, Basic Energy Sciences, Chemical Sciences, Biosciences, and Geosciences Division

(CSGB), Heavy Element Chemistry Program and was performed at Lawrence Berkeley National Laboratory under contract No. DE-AC02-05CH11231. CIP was supported by the Geosciences Group at Pacific Northwest National Laboratory. Tc K-edge XAFS spectra were obtained at the Stanford Synchrotron Radiation Lightsource, SLAC National Accelerator Laboratory, which is supported by the U.S. Department of Energy, Office of Science, Office of Basic Energy Sciences under Contract No. DE-AC02-76SF00515. STXM and XMCD data were obtained at Beamline 11.0.2 at the ALS, which is supported by the Director, Office of Science, Office of Basic Energy Sciences, CSGB Condensed Phase and Interfacial Molecular Sciences program, of the U.S. Department of Energy at Lawrence Berkeley National Laboratory under Contract No. DE-AC02-05CH11231. The ALS and TT are supported by the Director, Office of Science, Office of Basic Energy Sciences, of the U.S. Department of Energy under Contract No. DE-AC02-05CH11231.

Supplemental Information. XANES spectra, larger diffraction patterns, larger EXAFS spectra and detailed fitting results, and combined analytical data are given in the SI.

References

(1) Icenhower, J. P.; Qafoku, N. P.; Zachara, J. M.; Martin, W. J. The biogeochemistry of technetium: a review of the behavior of an artificial element in the natural environment. *Am. J. Sci.* **2010**, *310*, 721.

(2) Pilkington, N. J. The solubility of technetium in the near-field environment of a radioactive-waste repository. *J. Less Common Met.* **1990**, *161*, 203.

(3) Kunze, S.; Neck, V.; Gompper, K.; Fanghanel, T. Studies on the immobilization of technetium under near field geochemical conditions. *Radiochim. Acta* **1996**, *74*, 159.

(4) Ishii, T.; Sakuragi, T. Technetium in the environment. *Radioisotopes* **2006**, *55*, 485.

(5) *Yucca Mountain Repository License Application*, DOE/RW-0573, Rev. 0, U.S. Department of Energy, 2008.

(6) Mann, F. M.; Puigh, R. J.; Finfrock, S. H.; Khaleel, R.; Wood, M. I. *Integrated Disposal Facility Risk Assessment*, RPP-15834, CH2M Hill Hanford Group, Inc., 2003.

(7) *Performance Assessment for the Saltstone Disposal Facility at the Savannah River Site*, SRR-CWDA-2009-00017, SRR Closure & Waste Disposal Authority, 2009.

(8) *EPA facts about Technetium-99*, U.S. Environmental Protection Agency, 2014.
(9) Liu, D. J.; Yao, J.; Wang, B.; Bruggeman, C.; Maes, N. Solubility study of Tc(IV) in a granitic water. *Radiochim. Acta* **2007**, *95*, 523.
(10) Hess, N. J.; Xia, Y. X.; Rai, D.; Conradson, S. D. Thermodynamic model for the solubility of $TcO_2 \cdot xH_2O$(am) in the aqueous Tc(IV)-Na^+-Cl^--H^+-OH^--H2O system. *J. Solution Chem.* **2004**, *33*, 199.
(11) Gu, B. H.; Dong, W. M.; Liang, L. Y.; Wall, N. A. Dissolution of technetium(IV) oxide by natural and synthetic organic ligands under both reducing and oxidizing conditions. *Environ. Sci. Technol.* **2011**, *45*, 4771.
(12) Boggs, M. A.; Minton, T.; Dong, W. M.; Lomasney, S.; Islam, M. R.; Gu, B. H.; Wall, N. A. Interactions of Tc(IV) with humic substances. *Environ. Sci. Technol.* **2011**, *45*, 2718.
(13) Sekine, T.; Watanabe, A.; Yoshihara, K.; Kim, J. I. Complexation of technetium with humic acid. *Radiochim. Acta* **1993**, *63*, 87.
(14) Yalcintas, E.; Gaona, X.; Altmaier, M.; Dardenne, K.; Polly, R.; Geckeis, H. Thermodynamic description of Tc(IV) solubility and hydrolysis in dilute to concentrated NaCl, $MgCl_2$ and $CaCl_2$ solutions. *Dalton Trans.* **2016**, *45*.
(15) Migge, H. Simultaneous evaporation of Cs and Tc during vitrification-a thermochemical approach. *Mater. Res. Soc. Symp. Proc.* **1990**, *176*, 411.
(16) Lammertz, H.; Merz, E.; Halaszovich, S. Technetium volatilization during HLW vitrification. *Mater. Res. Soc. Symp. Proc.* **1985**, *44*, 823.
(17) Bibler, N. E.; Fellinger, T. L.; Marra, S. L.; O'Driscoll, R. J.; Ray, J. W.; Boyce, W. T. Tc-99 and Cs-137 volatility from the DWPF production melter during vitrification of the first macrobatch of HLW sludge at the Savannah River Site. *Mater. Res. Soc. Symp. Proc.* **2000**, *608*, 697.
(18) Lee, M.-S.; Um, W.; Wang, G.; Kruger, A. A.; Lukens, W. W.; Rousseau, R.; Glezakou, V.-A. Impeding ^{99}Tc(IV) mobility in novel waste forms. *Nature Commun.* **2016**, *7*, 12067.
(19) Ringwood, A. E.; Kesson, S. E.; Ware, N. G.; Hibberson, W.; Major, A. Immobilization of high-level nuclear reactor wastes in Synroc. *Nature* **1979**, *278*, 219.
(20) Muller, O.; White, W. B.; Roy, R. Crystal chemistry of some technetium-containing oxides. *J. Inorg. Nucl. Chem.* **1964**, *26*, 2075.
(21) Shannon, R. D. Revised effective ionic-radii and systematic studies of interatomic distances in halides and chalcogenides. *Acta Cryst. A* **1976**, *32*, 751.
(22) Edouminko, A.; Colin, F.; Trescases, J. J. Alterability of titanium minerals (ilmenite and rutile) and titanium mobility in the weathering profiles of the Ovala sector (Gabon). *J. Afr. Earth Sci.* **1995**, *21*, 313.
(23) Ramanaidou, E.; Nahon, D.; Decarreau, A.; Melfi, A. J. Hematite and goethite from duricrusts developed by lateritic chemical weathering of Precambrian banded iron formations, Minas Gerais, Brazil. *Clay Clay Miner.* **1996**, *44*, 22.
(24) Shuster, D. L.; Vasconcelos, P. M.; Heim, J. A.; Farley, K. A. Weathering geochronology by (U-Th)/He dating of goethite. *Geochim. Cosmochim. Acta* **2005**, *69*, 659.
(25) Yapp, C. J. Climatic implications of surface domains in arrays of SD and delta O-18 from hydroxyl minerals: goethite as an example. *Geochim. Cosmochim. Acta* **2000**, *64*, 2009.
(26) Skomurski, F. N.; Rosso, K. M.; Krupka, K. M.; McGrail, B. P. Technetium incorporation into hematite (alpha-Fe_2O_3). *Environ. Sci. Technol.* **2010**, *44*, 5855.

(27) Kobayashi, T.; Scheinost, A. C.; Fellhauer, D.; Gaona, X.; Altmaier, M. Redox behavior of Tc(VII)/Tc(IV) under various reducing conditions in 0.1 M NaCl solutions. *Radiochim. Acta* **2013**, *101*, 323.
(28) Um, W.; Chang, H. S.; Icenhower, J. P.; Lukens, W. W.; Serne, R. J.; Qafoku, N. P.; Westsik, J. H.; Buck, E. C.; Smith, S. C. Immobilization of 99-technetium (VII) by Fe(II)-goethite and limited reoxidation. *Environ. Sci. Technol.* **2011**, *45*, 4904.
(29) Um, W.; Chang, H.; Icenhower, J. P.; Lukens, W. W.; Serne, R. J.; Qafoku, N.; Kukkadapu, R. K.; Westsik, J. H. Iron oxide waste form for stabilizing Tc-99. *J. Nucl. Mat.* **2012**, *429*, 201.
(30) Pepper, S. E.; Bunker, D. J.; Bryan, N. D.; Livens, F. R.; Charnock, J. M.; Pattrick, R. A. D.; Collison, D. Treatment of radioactive wastes: an X-ray absorption spectroscopy study of the reaction of technetium with green rust. *J. Colloid Interface Sci.* **2003**, *268*, 408.
(31) Marshall, T. A.; Morris, K.; Law, G. T. W.; Mosselmans, J. F. W.; Bots, P.; Parry, S. A.; Shaw, S. Incorporation and retention of 99-Tc(IV) in magnetite under high pH conditions. *Environ. Sci. Technol.* **2014**, *48*, 11853.
(32) Smith, F. N.; Um, W.; Taylor, C. D.; Kim, D.-S.; Schweiger, M. J.; Kruger, A. A. Computational investigation of technetium(IV) incorporation into inverse spinels: magnetite (Fe_3O_4) and trevorite ($NiFe_2O_4$). *Environ. Sci. Technol.* **2017**, *50*, 5216.
(33) Bohor, B. F.; Foord, E. E.; Ganapathy, R. Magnesioferrite from the Cretaceous-Tertiary boudary, Caravaca, Spain. *Earth Planet. Sci. Lett.* **1986**, *81*, 57.
(34) Tang, Z. X.; Sorensen, C. M.; Klabunde, K. J.; Hadjipanayis, G. C. Preparation of manganese ferrite fine particles from aqueous solution. *J. Colloid. Interface. Sci.* **1991**, *146*, 38.
(35) Kodama, T.; Wada, Y.; Yamamoto, T.; Tsuji, M.; Tamaura, Y. Synthesis and characterization of ultrafine nickel(II)-bearing ferrites ($Ni_xFe_{3-x}O_4$, X=0.14-1.0). *J. Mater. Chem.* **1995**, *5*, 1413.
(36) Sugimoto, T.; Matijevic, E. Formation of uniform spherical magnetite particles by crystallization from ferrous hydroxide gel. *J. Colloid Interface Sci.* **1980**, *74*, 227.
(37) Kaneko, K.; Katsura, T. Formation of Mg-bearing ferrite by the air oxidation of aqueous suspensions. *Bull. Chem. Soc. Jpn.* **1979**, *52*, 747.
(38) Kiyama, M. Formation of manganese and cobalt ferrites by air oxidation of aqueous suspensions and their properties. *Bull. Chem. Soc. Jpn.* **1978**, *51*, 134.
(39) Wilson, A. D. The micro-determination of ferrous iron in silicate minerals by a volumetric and a colorimetric method. *Analyst* **1960**, *85*, 823.
(40) Whitehead, D.; Malik, S. A. Determination of ferrous and total iron in silicate rocks by automated colorimetry. *Anal. Chem.* **1975**, *47*, 554.
(41) Koningsberger, D. C.; Prins, R. *X-Ray Absorption: Principles, Applications, Techniques of EXAFS, SEXAFS, and XANES*; John Wiley & Sons: New York, 1988.
(42) Newville, M. IFEFFIT: interactive XAFS analysis and FEFF fitting. *J. Synchrotron Rad.* **2001**, *8*, 322.
(43) Ravel, B. ATHENA and ARTEMIS interactive graphical data analysis using IFEFFIT. *Phys. Scripta* **2005**, *T115*, 1007.
(44) Mustre de Leon, J.; Rehr, J. J.; Zabinsky, S. I.; Albers, R. C. Ab initio curved-wave x-ray-absorption fine structure. *Phys. Rev. B* **1991**, *44*, 4146.
(45) Bosi, F.; Halenius, U.; Skogby, H. Crystal chemistry of the magnetite-ulvospinel series. *Am. Mineral.* **2009**, *94*, 181.

(46) Downward, L.; Booth, C. H.; Lukens, W. W.; Bridges, F. A variation of the F-test for determining statistical relevance of particular parameters in EXAFS fits. *AIP Conf. Proc.* **2007**, *882*, 129.
(47) Bluhm, H.; Andersson, K.; Araki, T.; Benzerara, K.; Brown, G. E.; Dynes, J. J.; Ghosal, S.; Gilles, M. K.; Hansen, H. C.; Hemminger, J. C.; Hitchcock, A. P.; Ketteler, G.; Kilcoyne, A. L. D.; Kneedler, E.; Lawrence, J. R.; Leppard, G. G.; Majzlan, J.; Mun, B. S.; Myneni, S. C. B.; Nilsson, A.; Ogasawara, H.; Ogletree, D. F.; Pecher, K.; Salmeron, M.; Shuh, D. K.; Tonner, B.; Tyliszczak, T.; Warwick, T.; Yoon, T. H. Soft X-ray microscopy and spectroscopy at the Molecular Environmental Science beamline at the Advanced Light Source. *J. Electron Spectrosc. Relat. Phenom.* **2006**, *150*, 86.
(48) van der Laan, G.; Kirkman, I. W. The 2p absorption spectra of 3d transition metal compounds in tetrahedral and octahedral symmetry. *J. Phys. Condens. Matter* **1992**, *4*, 4189.
(49) van der Laan, G.; Thole, B. T. Strong magnetic X-ray dichroism in 2p absorption spectra of 3d transition metal ions. *Phys. Rev. B* **1991**, *43*, 13401.
(50) Pattrick, R. A. D.; Van der Laan, G.; Henderson, C. M. B.; Kuiper, P.; Dudzik, E.; Vaughan, D. J. Cation site occupancy in spinel ferrites studied by X-ray magnetic circular dichroism: developing a method for mineralogists. *Eur. J. Mineral.* **2002**, *14*, 1095.
(51) Pearce, C. I.; Henderson, C. M. B.; Pattrick, R. A. D.; Van der Laan, G.; Vaughan, D. J. Direct determination of cation site occupancies in natural ferrite spinels by L_2,L_3 X-ray absorption spectroscopy and X-ray magnetic circular dichroism. *Am. Mineral.* **2006**, *91*, 880.
(52) Liang, L. Y.; Gu, B. H.; Yin, X. P. Removal of technetium-99 from contaminated groundwater with sorbents and reductive materials. *Separ. Technol.* **1996**, *6*, 111.
(53) Cui, D. Q.; Eriksen, T. E. Reduction of pertechnetate by ferrous iron in solution: influence of sorbed and precipitated Fe(II). *Environ. Sci. Technol.* **1996**, *30*, 2259.
(54) Peretyazhko, T.; Zachara, J. M.; Heald, S. M.; Jeon, B. H.; Kukkadapu, R. K.; Liu, C.; Moore, D.; Resch, C. T. Heterogeneous reduction of Tc(VII) by Fe(II) at the solid-water interface. *Geochim. Cosmochim. Acta* **2008**, *72*, 1521.
(55) Peretyazhko, T.; Zachara, J. M.; Heald, S. M.; Kukkadapu, R. K.; Liu, C.; Plymale, A. E.; Resch, C. T. Reduction of Tc(VII) by Fe(II) sorbed on Al (hydr)oxides. *Environ. Sci. Technol.* **2008**, *42*, 5499.
(56) Zachara, J. M.; Heald, S. M.; Jeon, B.-H.; Kukkadapu, R. K.; Liu, C.; McKinley, J. P.; Dohnalkova, A. C.; Moore, D. A. Reduction of pertechnetate Tc(VII) by aqueous Fe(II) and the nature of solid phase redox products. *Geochim. Cosmochim. Acta* **2007**, *71*, 2137.
(57) Nguyen, T. K. T.; Maclean, N.; Mahiddine, S. Mechanisms of nucleation and growth of nanoparticles in solution. *Chem. Rev.* **2014**, *114*, 7610.
(58) Sasai, R.; Norimatsu, W.; Matsumoto, Y. Nitrate-ion-selective exchange ability of layered double hydroxide consisting of Mg-II and Fe-II. *J. Hazard. Mat.* **2012**, *215*, 311.
(59) Wang, Y.; Gao, H. Compositional and structural control on anion sorption capability of layered double hydroxides (LDHs). *J. Colloid. Interface. Sci.* **2006**, *301*, 19.
(60) Collyer, S.; Grimes, N. W.; Vaughan, D. J.; Longworth, G. Studies of the crystal-structure and crystal-chemistry of titanomaghemite. *Am. Mineral.* **1988**, *73*, 153.
(61) Berry, F. J.; Greaves, C.; Helgason, O.; McManus, J.; Palmer, H. M.; Williams, R. T. Structural and magnetic properties of Sn-, Ti-, and Mg-substituted alpha-Fe_2O_3: A study by neutron diffraction and Mossbauer spectroscopy. *J. Solid State Chem.* **2000**, *151*, 157.

(62) Berry, F. J.; Bohorquez, A.; Helgason, O.; Jiang, J. Z.; McManus, J.; Moore, E.; Mortimer, M.; Mosselmans, F.; Morup, S. An investigation of the local environments of tin in tin-doped alpha-Fe_2O_3. *J. Phys. Condens. Matter* **2000**, *12*, 4043.
(63) Berry, F. J.; Greaves, C.; Helgason, O.; McManus, J. Synthesis and characterization of tin-doped iron oxides. *J. Mater. Chem.* **1999**, *9*, 223.
(64) Berry, F. J.; Skinner, S. J.; Helgason, O.; Bilsborrow, R.; Marco, J. F. Location of tin and charge balance in materials of composition $Fe_{3-x}Sn_xO_4$ ($x<0.3$). *Polyhedron* **1998**, *17*, 149.
(65) Faggiani, R.; Lock, C. J. L.; Poce, J. Structure of ammonium pertechnetate at 295, 208 and 141 K. *Acta Crystallogr. Sect. B-Struct. Commun.* **1980**, *36*, 231.
(66) McGregor, D.; Burton-Pye, B. P.; Howell, R. C.; Mbomekalle, I. M.; Lukens, W. W.; Bian, F.; Mausolf, E.; Poineau, F.; Czerwinski, K. R.; Francesconi, L. C. Synthesis, structure elucidation, and redox properties of Tc-99 complexes of lacunary Wells-Dawson polyoxometalates: insights into molecular Tc-99-metal oxide interactions. *Inorg. Chem.* **2011**, *50*, 1670.
(67) Lukens, W. W.; Bucher, J. J.; Edelstein, N. M.; Shuh, D. K. Products of pertechnetate radiolysis in highly alkaline solution: Structure of $TcO_2 \cdot xH_2O$. *Environ. Sci. Technol.* **2002**, *36*, 1124.
(68) Pearce, C. I.; Henderson, C. M. B.; Telling, N. D.; Pattrick, R. A. D.; Charnock, J. M.; Coker, V. S.; Arenholz, E.; Tuna, F.; van der Laan, G. Fe site occupancy in magnetite-ulvospinel solid solutions: A new approach using X-ray magnetic circular dichroism. *Am. Mineral.* **2010**, *95*, 425.
(69) Pearce, C. I.; Qafoku, O.; Liu, J.; Arenholz, E.; Heald, S. M.; Kukkadapu, R. K.; Gorski, C. A.; Henderson, C. M. B.; Rosso, K. M. Synthesis and properties of titanomagnetite ($Fe_{3-x}Ti_xO_4$) nanoparticles: A tunable solid-state Fe(II/III) redox system. *J. Colloid Interface Sci.* **2012**, *387*, 24.
(70) Smith, P. P. K. Spinodal decomposition in a titanomagnetite. *Am. Mineral.* **1980**, *65*, 1038.
(71) Lilova, K. I.; Pearce, C. I.; Rosso, K. M.; Navrotsky, A. Energetics of spinels in the Fe-Ti-O system at the nanoscale. *Chem. Phys. Chem.* **2014**, *15*, 3655.
(72) Pearce, C. I.; Liu, J.; Baer, D. R.; Qafoku, O.; Heald, S. M.; Arenholz, E.; Grosz, A. E.; McKinley, J. P.; Resch, C. T.; Bowden, M. E.; Engelhard, M. H.; Rosso, K. M. Characterization of natural titanomagnetites ($Fe_{3-x}Ti_xO_4$) for studying heterogeneous electron transfer to Tc(VII) in the Hanford subsurface. *Geochim. Cosmochim. Acta* **2014**, *128*, 114.

611 TOC Figure:

612

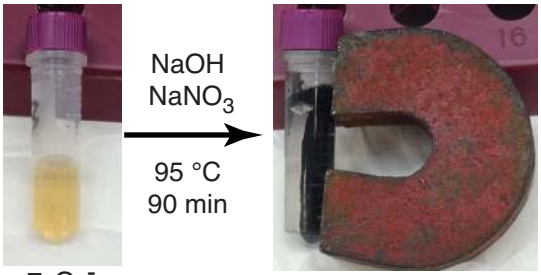

613

614

615

616

617

618